EFDA–JET–PR(11)62

G. Bonheure, M. Hult, R. González de Orduña, D. Arnold, H. Dombrowski,
M. Laubenstein, E. Wieslander, T. Vidmar, P. Vermaercke, C. Perez Von Thun,
M. Reich, S. Jachmich, A. Murari, S. Popovichev J. Mlynar, A. Salmi,
O. Asunta, M. Garcia- Munoz, R. Koslowski, S. Kragh Nielsen
and JET EFDA contributors

Experimental Investigation of $d(^3He,p)\alpha$ and d(d,p)t Fusion Reaction Products Confinement in JET

Experimental Investigation of d(^{3}He,p)α and d(d,p)t Fusion Reaction Products Confinement in JET

G. Bonheure[1], M. Hult[2], R. González de Orduña[2], D. Arnold[3], H. Dombrowski[3], M. Laubenstein[4], E. Wieslander[2,13], T. Vidmar[5], P. Vermaercke[5], C. Perez Von Thun[6], M. Reich[6], S. Jachmich[1], A. Murari[7], S. Popovichev[8], J. Mlynar[9], A. Salmi[10], O. Asunta[10], M. Garcia-Munoz[6], R. Koslowski[11], S. Kragh Nielsen[12] and JET EFDA contributors*

JET-EFDA, Culham Science Centre, OX14 3DB, Abingdon, UK

[1]ERM-KMS, B-1000 Brussels, Belgium, Partner in the Trilateral Euregio Cluster
[2]European Commission, Joint Research Centre, Institute for Reference Materials and Measurements (IRMM), Retieseweg 111, B-2440 Geel, Belgium
[3]Physikalisch-Technische Bundesanstalt (PTB), Bundesallee 100, 38116 Braunschweig, Germany
[4]Laboratori Nazionali del Gran Sasso, S.S. 17/bis km 18+910, I-67010 Assergi (AQ), Italy
[5]SCK•CEN, Boeretang, B-2400 Mol, Belgium
[6]Max-Planck-Institut für Plasmaphysik, EURATOM-Assoziation, D-85748 Garching, Germany
[7]Association EURATOM/ENEA, Consorzio RFX, 4-35127 Padova, Italy
[8]URATOM-CCFE Fusion Association, Culham Science Centre, OX14 3DB, Abingdon, OXON, UK
[9]Association EURATOM-IPP.CR, CZ-182 21 Prague 8, Czech Republic
[10]Helsinki University of Technology, Association EURATOM-Tekes, P.O.Box 4100, FIN-02015 TKK, Finland
[11]Forschungszentrum Jülich GmbH, Institut für Plasmaphysik, EURATOM-Assoziation, Trilateral Euregio Cluster, D-52425 Jülich, Germany
[12]Risø DTU, 4000 Roskilde, Danemark
[13]CTBTO Preparatory Commission, P.O Box 1200, 1400 Vienna
** See annex of F. Romanelli et al, "Overview of JET Results", (23rd IAEA Fusion Energy Conference, Daejon, Republic of Korea (2010)).*

Preprint of Paper to be submitted for publication in
Nuclear Fusion

ABSTRACT

In ITER, magnetic fusion will explore the burning plasma regime. Because such burning plasma is sustained by its own fusion reactions, alpha particles need to be confined [1]. New experiments using d(^{3}He,p)α and d(d,p)t fusion reaction products were performed in JET. Fusion product loss was measured from MHD-quiescent plasmas with a charged particle activation probe installed at a position opposite to the magnetic field ion gradient drift (see in figure 1) - 1.77m above mid-plane - in the ceiling of JET tokamak. This new kind of escaping ion detector [6] provides for absolutely calibrated measurements. Both the mechanism and the magnitude of the loss are dealt with by this research. Careful analysis shows measured loss is in quantitative agreement with predictions from the classical orbit loss model. However, the comparison with simulated loss radial profile, although improved compared to previous studies in TFTR, Princeton, US, [2] is not fully satisfactory and potential explanations for this discrepancy are examined.

1. INTRODUCTION

One fundamental issue for fusion reactors and future large scale fusion experiments in ITER is the behaviour of the large alpha particle population (3.5MeV). These alpha particles produced in D-T fusion reactions must be confined. A crucial aspect of alpha particle physics is the fraction of alphas lost to the first wall. First, loss of alpha particles prior to their thermalization causes a significant decrease of the self heating power available to achieve ignition. Second, it is necessary to predict alpha particle loss to the first wall and divertor plates since it may cause damage and reduce their lifetime. Finally, studies of alpha particle loss mechanism could also prove valuable in developing methods of helium ash removal, burn control and alpha channelling[1].

Research progress in the field of alpha particles and energetic particle physics [48,49] has traditionally been driven by theory. In recent years, progress was accomplished in the area of energetic particle simulations. State-of-the art calculations of fast ion fluxes and power loads to the plasma-facing components in ITER are now readily available [10]. By contrast, few experimental investigations have attempted to validate the theoretical model predictions, essentially because of the lack of accurate measurement techniques. Diagnosing alpha particles in reactor-scale fusion plasmas remain challenging[11]. Detectors capable of operating in the harsh environment of the ITER first wall need further development and a range of measurement techniques may be necessary to meet the demands of ITER[12] and future fusion devices.

Orbit loss of alpha particles is generally well understood. It was investigated in many previous experiments [2-4, 55-58] such as in alpha particle physics experiments in TFTR. The results from these remarkable experiments present, however, a complex pattern which is not fully understood. Anomalous results were reported from a detector 90^o below the mid-plane and radial profile results from the mid-plane detector were found inconsistent with modeling [2]. Note in these TFTR experiments[4], absolute calibration of the lost alpha scintillators was not a routine procedure. Similarly, accurate comparisons between model and experiments have so far not yet been performed

in JET because of these aforementioned difficulties of i) performing such measurements in large tokamaks and ii) calibrating the measurements.

This paper presents new experimental evidence pertaining to d(^{3}He,p)α and d(d,p)t fusion reaction products and, to the authors knowledge, the first attempt in JET to validate first loss models with accurate flux measurements at the wall. During these JET experiments, fusion product loss was measured from MHD-quiescent plasmas using a charged particle activation probe that was operated at a position - 1.77m above mid-plane - in the JET ceiling. This new kind of escaping ion detector[6] provides for well calibrated data at a new measuring point (see in figure 1), where no previous experimental data are available.

The paper is organized, as follows, the measurement techniques are discussed in section 2. Section 3 presents the model used to calculate alpha loss. In section 4, the results are examined. Experimental data are compared with the orbit alpha loss model, the results are discussed and, in section 5, summary and conclusions are given.

2. DIAGNOSTICS

2.1 MEASUREMENT TECHNIQUES

Direct charged particle detection in the fusion product energy range (e.g 3.6MeV for alpha particle) relies only on two fundamental interaction processes [18,19]: i) inelastic scattering on atomic electrons and ii) nuclear reactions. Conventional detection methods – semiconductor detectors, gas detectors, scintillation detectors - are based on the first process, interaction with electrons.

In the environment of a fusion reactor - ITER expected numbers[20,53] for alpha particles and neutron flux densities are up to $10^{18}\,m^2s^{-1}$ and $10^{19}\,m^2s^{-1}$ respectively, plasma radiation: $500kWm^{-2}$ - the performance and reliability of the former techniques are questionable. Shielding space is limited due to particle orbit constraints and detector saturation is likely to arise from the huge background radiation. Detector background in the neutron gamma n/γ radiation field is mainly due to Compton electrons absorption which is weakly dependent on the detector and shield cover material chosen.

Most of the results presented in this paper are obtained using a charged particle activation probe, a new kind of escaping ion detector that is based on the above mentioned second fundamental process [6]. The primary advantages of this technique which is described in section 2.2 are:

(i) Due to its absolute calibration and accuracy, it provides a valuable cross calibration for the other lost alpha detectors and validation of alpha loss models

(ii) Its improved particle identification and energy resolution capability

(iii) Its immunity to electromagnetic, mechanical noise, to heat and high radiation flux and a high signal to noise ratio.

The latter may prove particularly useful in view of applications to ITER[36] and future fusion reactors.

In the JET tokamak, fast ion loss is also measured with a 20 micron thin scintillator plate of the P56 type (Y_2O_3:Eu^{3+}) [35], see in figure 1 for the position. The temporal evolution of 2-D

distributions as function of Larmor radius and pitch angle of co-circulating fast particles can be measured with this technique (see in figure 7). More details on this diagnostic are given in [9]. Indirect measurement methods have been developed including current Faraday Cups (FC) [21], mass [22] or heat measurements [23,24] . FC is the most developed one so far. A set of ten faraday cup detectors with a 1 millisecond time resolution is mounted inside the JET vacuum-vessel (see in figure 1 for the position). This instrument is described in [50, 7] and the most recent progress in the faraday cups are reported in [39, 40]. Finally, gammaray [25, 26] and neutron diagnostics [27] are important diagnostic tools in these experiments in order to monitor the confined fusion products and the D-D neutron emission.

2.2 ACTIVATION PROBE

Based on nuclear reactions, the charged particle activation method is a novel concept recently tested in JET [6]. It consists of an activation probe made of a holder and activation samples. For this experiment, 45 samples in total were placed in a holder made of Boron-Nitride (BN) with a hexagonal cross section (see figure 2). The holder was mounted at the lower end of a manipulator arm system located in the JET ceiling (See in figure 1). On each of the six sides, the holder has a slot in which to place the samples. The distribution of the samples in the BN probe, together with their thickness and length is presented in Table 1. The notation of the samples consists of a letter indicating the compound, followed by a number indicating the slot, and therefore the orientation (see in figure 2), and a second number indicating the row.

For the samples that were placed in stacks, the third number indicates the position of the sample in the stack (1 corresponds to the top surface-level sample). All the slots were 10mm wide. The vanadium surface foils were 10×50mm and covered almost an entire slot, apart from the rounded tip of the TVA samples. The upper part of the holder was covered by a carbon tube.

All samples were of natural isotopic abundance. The sample responses were studied in details and calculated with the FISPACT code [29]. Activation coefficients calculated with FISPACT for several of the sample materials irradiated by protons at different proton energies are plotted in figure 3. The position of 3MeV D-D protons and 14.7MeV D-^{3}He protons is indicated by an arrow on the energy axis.

2.3 ULTRA LOW LEVEL GAMMA RAY SPECTROMETRY

Ultra Low level Gamma ray Spectrometry (ULGS) is required in order to analyze the activation probe samples because of the low sample activity in the milli-Becquerel range [30]. ULGS is best performed in underground laboratories. The background measured in underground laboratories is up to 105 lower compared to a standard above-ground detector. A detailed gamma-ray spectrometry analysis of each individual sample was performed at the following facilities:

1) IRMM (Institute for Reference Materials and Measurements) in the 225m deep underground laboratory HADES located at the Belgian nuclear centre SCK•CEN in Mol, Belgium [31],

2) PTB in the underground laboratory UDO located at a depth of 490 m in the ASSE salt mine close to Braunschweig, Germany [32]
3) Laboratori Nazionali del Gran Sasso (LNGS) in the 3800 water meter equivalent (mwe) low background counting facility located in the Gran Sasso nearby Assergi in Italy[33].

Previous experience with activation technique[18,28] shows the presence of impurities may explain unexpected radionuclides in the samples, and may interfere with the actual measurements. For this reason, the impurities of one sample of each type were carefully determined by neutron activation analysis (k_0-NAA) [34] at SCK•CEN in Mol. For details on the results, see in [47, 54]. This experimentally determined composition is taken into account in the FISPACT calculation in order to provide the most accurate value for the activation coefficients.

3. FIRST ORBIT LOSS MODEL

First orbit loss is the loss associated with particles born on orbits that intersect the wall on their first poloidal transit. These particles are lost with their birth energy since the time for one bounce (<10microseconds) and their loss is much less than the collisional slowing down time of several hundreds milliseconds. The global fraction of fast particles that are first orbit lost decreases with increasing plasma current. This is due to the reduced banana width of trapped particles at higher current, resulting in a particle staying closer to a given flux surface and thus further away from the walls.

Two methods to determine the first orbit losses at a detector wall location are usually followed:

1) In the first one, a forward method, forward propagation of a packet of initial conditions is performed using adequate Monte Carlo techniques [10, 41]. The particles are then followed by numerically integrating their equation of motion, assuming a steady state plasma background. In order to obtain the most accurate results, 3-dimensionnal vacuum magnetic field and 3-dimensionnal wall maps must be used in these simulations. In this method, many particles are followed (typically ~105 particles) but few of them reach the desired wall location. Because of the need to follow a large number of particles to reach sufficient statistical accuracy, these simulations do not take into account the full 3-D (Larmor) orbits. Instead, particles are followed by numerically integrating their guiding-centre equation of motion.
2) This difficulty may be removed by setting initial conditions of virtual particles at the detector wall location and by following their full Larmor orbits, backward into the plasma. This second method, which is followed in this paper, is more efficient to determine the response of a wall detector to the first orbit losses.

The ASCOT code [41] is one of the most powerful tool developed to perform guiding–center following Monte Carlo simulations in fusion devices. It was used recently to predict alpha particle wall loads for ITER[10]. More information about the ASCOT code can be found in the latter two references.

3. 1 DETECTION EFFICIENCY

The method followed in this paper was originally developed for experiments at the PLT tokamak [43]. This method is based on phase space volume conservation due to an invariant property of the equation: the motion of collisionless fast ions in the plasma is Hamiltonian.

$$m\,\frac{d\bar{v}}{dt} = q\bar{v}\times\bar{B} \tag{1}$$

The detection efficiency is defined as the ratio of the number of detected particles to the total number of particles emitted by the source. It is the product of the detector intrinsic efficiency and the geometric etendue. The detector intrinsic efficiency is given in previous section 2.2. Let us now consider the geometric efficiency which depends on the position of the detector and the geometry and position of the particle source $S_{E_0}(\vec{r}, \vec{\Omega})$ and the trajectories of particles from the plasma to the detector.

The ratio of the number of detected particles to the total number of particles emitted by the source, referred here as the efficiency ε, is expressed as [43]:

$$\varepsilon = \frac{\int_{S_D} dA_D \int_{Ap} d\Omega_D T(\theta)\cos(\theta) \int_{Orbit} S_{E0}(\vec{r},\vec{\Omega})dl}{\int dA_p\, dl \int d\Omega\, S_{E0}(\vec{r},\vec{\Omega})} \tag{2}$$

where the subscript 'orbit' in the integral in equation (2) means that the integration has to be calculated along the full orbit of the particle and along all possible paths to the detector. T(θ) is the transmission function of the detector aperture. Expression (2) above is calculated numerically with a full orbit code for each relevant particle momentum and magnetic field. For all the initial velocities allowed by the detector aperture geometry, trajectories are followed from the detector to the plasma. In this work, the trajectories are calculated using an adapted version of Gourdon Code [44] for JET geometry and EFIT equilibrium [45]. These trajectories explore a four-dimensionnal phase space ε (r, z, ϕ, β) where β is the absolute value of the pitch angle expressed as:

$$\beta = \frac{|\vec{v}\times\vec{B}|}{|\vec{v}||\vec{B}|}$$

while (r, z, ϕ) are the space coordinates in the plasma: major radius, vertical coordinate and toroidal angle respectively. The detection efficiency distribution is plotted in figure 6 for 14.6MeV protons and JET Pulse No: 72624 with time-integration from 6 to 13s. Because of the detector position - opposite to the magnetic field ion gradient drift- (figure 1), most of the plasma is invisible to the detector and only particles emitted in the plasma periphery as shown in figure 6 reach the detector.

3. 2 SOURCE PROFILE MODEL

The main fusion reactions in the plasma are the following:

$$D + {}^3He \rightarrow p\ (14.7MeV) + \alpha\ (3.7MeV) \tag{3}$$

$$D + D \rightarrow p\ (3.0MeV) + T\ (1.0MeV) \quad (4)$$

$$D + D \rightarrow n\ (2.5MeV) + {}^{3}He\ (0.8MeV) \quad (5)$$

$$D + T \rightarrow n\ (14.1MeV) + \alpha\ (3.6MeV) \quad (6)$$

The Larmor radii of the charged fusion products are given in the table 2 at the minimum and maximum toroidal field values in these experiments.

4. RESULTS

The activation probe was exposed to a total of 10 JET plasma pulses (see in table 3). All plasmas were in D-^{3}He fuel mixture up to n (^{3}He) / n_e ~ 20% in ^{3}He concentration except for the first reference plasma in pure deuterium. In these plasmas, the toroidal magnetic fields were 2.2 to 3.45T and plasma currents were 1.5 to 2.2MA. Plasmas were heated with deuterium Neutral Beam Injection NBI (D) only with up to 19MW heating power and with total cumulated duration of 100s for the 10 pulses. Plasmas conditions were carefully controlled to avoid any strong MHD activity. The total number of neutrons measured by the fission chambers and summed over all plasmas was 3.2×10^{17} (with an uncertainty of ±10%). The D-D emission in each individual pulse is given in table 3 (see in 5th column) as well as the relative intensity of 16.6MeV emission (see in last column) from the weak branch of the D-3He fusion reaction.

The conditions for this new experiment are much improved compared to the previous study. In the previous experiment[6], the samples were exposed for four consecutive days and were irradiated in a total of 63 JET plasma pulses. They were exposed to a wide range of plasma heating schemes while in the here reported experiment the samples were exposed to pure deuterium neutral beam injection NBI (D) heating which simplify the study. Furthermore, there was less variation in the fuel mixture and the plasma current: 1.5 to 2.5MA in the previous experiment compared to 1.5 to 2.2MA in this experiment. The total number of neutrons measured by the fission chambers [27] and summed over all plasmas was 5.08×10^{17} (with an uncertainty of ±10%) for the previous experiment compared to 3.2×10^{17} (with an uncertainty of ±10%) in this experiment.

4.1 MEASURED ACTIVITIES

Results, presented in this section, are given for all the measured activities of charged particle induced products found in the 45 samples. As expected, a few activation products induced by 2.5MeV and 14MeV neutrons from fusion reactions (5) and (6), see in section 3, are also found. These activation products are not included in the table 5 below as the paper scope is limited to the analysis of charged fusion products. Proton activation observed in the first JET experiment [6] with D-^{3}He plasmas was largely confirmed in this second experiment. The comparison to the previous results shows the following improvements:

i) Detection of seven radionuclides produced by proton interactions compared to two in the former experiment.

ii) Protons were detected in 28 samples compared to 8 samples in the former experiment. iii) the irradiation duration of only 6.5 hours (time between first and last pulse) is short in comparison to the shortest half-live measured (78h) such that timing of each individual pulse can be neglected.

4.2 MEASURED FUSION PRODUCT LOSS FROM D(^{3}He,P)A REACTION

As mentioned in section 2, several diagnostics were available to measure the fusion product loss during this JET experiment. Due to some noise issue during the experiment, however, no reliable data could be obtained from the faraday cups. Data is available from the scintillator for each pulse (see in table 3). This data confirms the loss of charged fusion products from these plasmas. Morover, the measured Larmor radius and pitch angle distributions are typical of prompt losses (see in figure 4). The accumulated (time-integrated) scintillator light which is roughly proportional to the alpha loss is given in the fourth column of table 4. Note the large drop of the scintillator light for Pulse No: 72634 is not fully understood. In the lowest toroidal field case, part of the signal was missing because of the Larmor radius exceeding the maximum value for the scintillator. Data for Pulse No: 72624 (B_t = 3.0T, I_P = 1.8MA) is shown in figure 7 time-integrated between 6.025s and 13.025s.

In the following, D-D fusion emission profile and D-^{3}He fusion emission are assumed to have quasi similar profile shape. This assumption is confirmed by calculations and reported in [46]. Using the detector responses of section 2.1, the 14.6MeV proton flux is unfolded assuming a mono-energetic spectrum for the protons. Our analysis showed the width of the experimental D-^{3}He spectrum due to beam-plasma reactions has a small effect on the activation distribution in the 5 sample stacks[47] and the assumption of a mono-energetic spectrum for the protons is justified.

The values obtained are reported in the table 5 below. In the first column, the detector for which the flux is calculated is specified, see table 1 and figure 2 for identification and position of the detector. In the second column, the product is given with its half-life. The main pathway for the radionuclide production is given in the third and the 14.6MeV energy proton fluence is given in the fourth column.

The highest proton flux is for the TV111 detector. It is the detector that is radially the nearest to the plasma. The same result was found in the first experiment. The maximum detected loss of fusion product is about 3 times higher in this experiment: $(1.43 \pm 0.11)\ 10^9\ cm^{-2}$ compared to $4.10^8\ cm^{-2}$ in the first experiment.

Note, ^{103}Pd, a proton induced product was initially inferred from the observation of X-ray peaks at 20 and 22keV on two rhodium detectors. However, these results could not be confirmed [47] and were not included in the following analysis.

In figure 8, the simulation of pitch angle distribution of orbit loss is plotted and compared to experimental data (see in figure 1 and figure 2 for ψ_V the orientation of the activation detectors with

respect to the tokamak). The data from the activation probe include a complete angular distribution of $^{48}V(t_{1/2= 15.98d})$ activation as well as data from single angular position from other proton produced products. A strong anisotropy is clearly seen with a maximum at the sample facing the inboard radial direction as expected from the proton trajectories. Note also, about 50% more protons hit sample 2 (protons travelling toroidally in the direction of the plasma current) compared to sample 6 (protons travelling toroidally in the direction opposite of the plasma current). Note the good agreement between the orbit loss model and experimental data.

The radial profile of proton orbit loss is simulated and compared with the experimental data in figure 9. An ASCOT source profile shape and a detection efficiency as detailed in section 3 are used in the simulation. The experimental data show a sharp decrease by a factor of ~50 for a radial shift of 4 cm. The tip of the probe is 15 cm away from the plasma and slightly behind mushroom limiters (see in figure 5b). Note the model over-predicts the number of particles at the detectors which are located further away from the plasma. We found that points at 4cm and 5cm away from the tip of the probe could not be modelled correctly even with significant alteration of the source profile shape. This suggests that the particles may be stopped before actually reaching the detectors further away from the plasma. Note, in this initial study, a 2-D poloidal wall boundary was used without taking into account the details of limiters.

The total $d(^3He,p)\alpha$ fusion reaction yield is estimated using the measured absolute value of the detected flux of 14.6MeV protons, given the ASCOT source profile and the detection efficiency calculated in section 3. The total $d(^3He,p)\alpha$ fusion reaction yield summed over all pulses (see table 4) is $2.5 +- 0.5\ 10^{16}$ and the average fuel ratio $n(^3He)/n_{(D)}$ is $8.6 +- 1.8\%$ which is acceptable, bearing in mind the measurement values of the same order obtained with the CXRS diagnostic

.

4.3 ALPHA PARTICLES

As mentioned above , the 3.7 MeV alpha particle, the second charged particle product of the $d(^3He,p)\alpha$ fusion reaction is, in favourable cases, detected by the mid-plane scintillator. Unfortunately, detection of the 14.6 MeV proton is not possible due to its huge Larmor radius (see in table 3 for typical Larmor radii of charged fusion products). By contrast, the activation probe is an instrument that may in principle detect a very large range of Larmor radii. For consistency of the results, the 3.7MeV alpha particle loss measured by the activation probe is now examined. It is entirely possible that some alpha particles are registered through the reaction Ti(a,n)Cr-51 on titanium-vanadium sample (see in table 5). However, Cr-51 is also produced through the V(p,n)Cr-51 reaction which has a higher cross section than the **Ti(α,n)Cr-51**. The most suitable activation probe sample that detects unambiguously alpha particle is the vanadium foil V1 through the V(α,n)Mn-54 nuclear reaction. The observation of Mn-54 in the vanadium foil V1 would give direct information on the loss of 3.7MeV alpha particles. The yield of this reaction is rather low, however, several factors are favourable for detecting this radionuclide: i) the high isotopic abundance of V-51 : 99.76%, ii) the half-life of Mn-54 is 312 days, iii) the g-ray energy of 835 keV is in a favourable spectrum

region with low background and iv) the γ-ray emission probability of the 835keV line is 99.975%. The V1 sample was measured in the HADES underground laboratory (see in chapter 2) for 2 weeks and the value obtained for the decision threshold is 190 microBecquerels. Therefore, the 3.7MeV alpha particle flux must be below a corresponding threshold value of ~ 3.6 10^9 cm^{-2}. The calculations of the 3.7MeV alpha particle detection efficiency give values at best ~ 19 times smaller than detection efficiency for 14.6MeV protons. This lower efficiency is easily understood because of the smaller Larmor radius of the 3.7MeV alpha particle compared to 14.6MeV protons (see table 3) . Consequently, given orbit loss simulation and given experimental data obtained in this experiment for the 14.6MeV high energy protons, the simulated flux of alpha particles is below the detectable limit (see table 7). Note however that if the activation probe position was near mid-plane poloidal position of the scintillator where the loss of fusion product is larger by about 2 orders of magnitude, alpha particle loss could be detected directly and quantified together with the 14.6MeV high energy protons.

4.4 d(d,p)t FUSION REACTION PRODUCTS

Activation data for the 19 samples placed in sample stacks at five locations of the activation probe – see in figure 2 – were carefully anayzed and the results were reported recently [47]. These results demonstrates both protons from the d(^{3}He,p)α and d(d,p)t fusion reactions are detected simultaneously and measured separately using a stack of thin layered detectors. The detection efficiency for the 3.024MeV proton is ~ 39 times lower than for the 14.6MeV high energy protons. The measured flux of 3.024MeV protons is shown in table 7 and is compared with the calculated flux from orbit loss, using the D-D fusion reaction profile shape from ASCOT and the total measured D-D neutron yield. The results demonstrate the good quantitative agreement between the orbit loss model and experimental data.

CONCLUSIONS

New measurements of the loss of d(3He,p)a and d(d,p)t fusion reaction products were performed in a JET experiment in plasmas with D-3He fuel mixture with up to 20% in ^{3}He concentration n(^{3}He)/n($_D$). Plasmas conditions were carefully controlled to avoid any strong MHD activity. Promptly lost 14.6 MeV high energy protons produced in d(^{3}He,p)α fusion reaction were detected. Absolute values for the loss of these energetic particles was measured with better than 10% accuracy. The pitch angle distribution and the radial profile of the loss were measured as well.

Loss of these energetic particles was calculated using the classical orbit loss mechanism at detector location. The measured flux of unconfined 14.6MeV high energy protons time - integrated over 100 seconds of plasma operation with high power NBI (D) heated plasmas does not exceed the level expected from classical orbit loss. Furthermore, the measured pitch angle distribution was found in good agreement with simulation. Loss of 3.024MeV protons from the d(d,p)t fusion reaction was measured as well and found in agreement with the orbit loss prediction.

Previous research on magnetic fusion product confinement has usually shown transport of energetic particles, unlike thermal transport, is not strongly determined by diffusion or turbulence. This new research corroborates this broad picture and suggests that in the case of MHD-quiescent plasmas, straightforward energetic particle orbit following simulation methods are sufficiently adequate to reproduce the measurements and to predict the fraction of fusion product loss.

In this initial study, a 2-D poloidal wall boundary was used without taking into account the details of limiters and this limitation may be the main cause for the discrepancy between the measured and simulated radial profile. The 3.7MeV alpha particles produced in the $d(^3He,p)\alpha$ fusion reactions could not be directly detected by the activation probe. However, an upper limit for the unconfined alpha particle flux was determined from ultra low level gamma ray spectrometry and was found consistent with the simulated alpha loss. Finally, alpha particle loss would be better quantified if the activation probe was installed near the mid-plane as the flux would be above the detection threshold.

ACKNOWLEDGEMENTS:

The contributions of all team members of IRMM, PTB and Gran Sasso are gratefully acknowledged. The authors would like to thank J. Vince, M. Stamp, G. Matthews, G. Kaveney, T. Edlington and the JET plasma boundary group for their continuous support. This work, supported by the European Communities under the contract of Association between EURATOM and Belgian state, was carried out within the framework of the European Fusion Development Agreement. The views and opinions expressed herein do not necessarily reflect those of the European Commission.

REFERENCES

[1]. Hazeltine R.D 2010 Fusion Engineering and Design **7-9** 85
[2]. Zweben S.J et al, 1999 Nuclear Fusion **40** 91
[3]. Boivin R. et al, 1992 Nuclear Fusion **33** 93 449
[4]. Darrow D. et al, 1995 Review of Scientific Instruments **66** 476
[5]. Sharapov S. et al, UKAEA FUSC 7841, October 2009. 11th IAEA Technical Meeting on Energetic Particles in Magnetic Confinement Systems, Kyiv, Ukraine
[6]. Bonheure G. et al 2008 Fusion Science and Technology **53** 3 806
[7]. Darrow D. et al 2006 Review of Scientific Instruments **77** 10 701
[8]. Reich M. et al, 33rd EPS Conference on Plasma Physics, Roma, Italy, June 19-23, 2006, P-2.131(European Physical Society, 2006) Conference Proceedings
[9]. Garcia-Munoz M. et al 2009 Review of Scientific Instruments **80** 5 3503
[10]. Kurki Suonio T. et al 2009 Nuclear Fusion **49** 095001
[11]. Donne A.J.H et al 2007 Nuclear Fusion **47** S337-S384
[12]. Costley A. et al 2009 IEEE doi: 10.1109/ANIMMA.2009.5503733
[13]. Esposito B. et al 1999 Review of Scientific Instruments **70** 1130
[14]. Sadler G. et al 1990 Review of Scientific Instruments **61** 3175

[15]. Batistoni P. et al 1987 Nuclear Fusion **27** 6 1043
[16]. Pillon M. et al 1990 Fusion Engineering IEEE 13th Symposium 160
[17]. Jarvis N. et al 1991 Fusion Technology **20** 265
[18]. Bonheure G. et al Physica Scripta **75** (2007) 769-773
[19]. Leo W. 'Techniques for nuclear and particle physics experiments', Springer, 1994
[20]. A.E. Costley et al., "ITER R&D: auxiliary systems: plasma diagnostics," Fusion Engineering and Design **55**, 331 (2001)
[21]. Jarvis O.N. et al 2001 Fusion Technology **39** 84
[22]. Herrmann H.W. et al 1997 Nuclear Fusion **37** 3 293
[23]. Bush C.E et al 1988 Review of Scientific Instruments **59** 8 1869
[24]. Tobita K. et al 2003 Fusion Engineering and Design **65** 561–8
[25]. Kiptily V et al 2006 Plasma Physics and Control Fusion 48 R59
[26]. Tardocchi M. et al 37th EPS Conference on Plasma Physics, Dublin, Ireland, 21-25 June, 2010, O4.119(European Physical Society, 2010) Conference Proceedings
[27]. Bonheure G. et al 2006 PoS(FNDA2006)091. Proceedings of Science. Trieste : SISSA (International School for Advanced Studies), 2005. ISSN 1824-8039. [http://pos.sissa.it/archive/conferences/025/091/FNDA2006_091.pdf] [International Workshop on Fast Neutron Detectors and Applications. University of Cape Town, South Africa (ZA), 03.04.2006-06.04.2006]
[28]. Bonheure G. et al, Review of Scientific Instruments **79**,1 (2008)
[29]. Forrest R.A. 2007 UKAEA FUS **534**
[30]. Gasparro J. et al 2006 Applied Radiation and Isotopes **64** (10-11) 1130
[31]. Hult M. et al 2000 Applied Radiation and Isotopes **53** (1-2) 225-229
[32]. Neumaier S et al 2000 Applied Radiation and Isotopes **53** (1-2) 173-178
[33]. Arpesella C. et al 1996 Applied Radiation and Isotopes **47** 991
[34]. Etxebarria N. et al 1996 Proceedings of the Second International k0-Users Workshop, Ljubljana, Slovenia. pp. 137-141.
[35]. Kajiwara K. et al 2003 J.Vac.Sci.Technol B **21**, 1622
[36]. Bonheure G. et al, Fusion Engineering and Design **86** (2011) 1298
[37]. Nishiura M. et al 2010 Review of Scientific Instruments **81** 10 313
[39]. Darrow D. et al 2010 Review of Scientific Instruments **81** 10 330
[40]. Cecil E. et al 2010 Review of Scientific Instruments **81** 10 326
[41]. J.A Heikkinen et al 1995 Physics of Plasmas **2** 3724-33
[42]. O.N. Jarvis et al 1996 Nuclear Fusion **36** 1513
[43]. Heidbrink, W.W et al, PhD Thesis, Princeton University (1984), chapter 2
[44]. Gourdon C. 'Programme optimise de calcul numérique dans les configurations magnétiques, Centres d'études nucléaires de Fontenay aux Roses' (1970)
[45]. Lao L.L et al 1985 Nuclear Fusion **25** 1421

[46]. Goloborodko V."Fokker-Planck Modelling of NBI Generated Deuterons in Tokamaks", 11th IAEA TCM on Energetic Particles, Kiev, 21-23 September (2009)
[47]. González de Orduña R et al 2011 Nuclear Instruments and Methods in Physics Research A 632 89–100
[48]. Breizman B.N and Sharapov S.E 2011 Plasma Physics and Controlled Fusion **53** 054001
[49]. Günter S. et al 2007 Nuclear Fusion **47** 920
[50]. Darrow D. et al 2004 Review of Scientific Instruments **75** 3566
[51]. Asunta O. et al, IAEA EP, Austin, 7-10.9 2011
[52]. The Stopping and Range of Ions in Matter, http://www.srim.org/
[53]. G. Vayakis et al., "Chapter 12: Generic diagnostic issues for a burning plasma experiment," Fusion Science and Technology. **53**(February 2008), 699–750
[54]. White R.B et al, Physics of Plasmas **3** (1996) 3043
[55]. Redi M.H et al, Physics of Plasmas **4** (1997) 4001
[56]. Medley S.S. et al, Plasmas Physics and Controlled Fusion **38** (1996) 1779
[57]. Heidbrink W.W. et al 1994 Nuclear Fusion **34** 535

Row number (height)	Slot 1 (0°)	2 (60°)	3 (120°)	4 (180°)	5 (240°)	6 (300°)
6 (44 mm) Top	T16(1.0)	T26(1.0)	T36(1.0)	T46(1.0)	T56(1.0)	T66(1.0)
5 (10 mm)		L 25(1.0)	B35(1.0)	W 45(1.0)		
4 (10 mm)		B 24(1.0)	B 34(1.0)	W 44(1.0)		
3 (10 mm)	Co stack	L stack			Rh stack	Y stack
	C121 (0.2)	L 231 (0.2)	B 33(1.0)	L 43(1.0)	R521 (0.1)	Y621(0.15)
	C122 (0.2)	L 232 (0.2)			R522 (0.1)	Y622(0.15)
	C123 (0.2)	L 233 (0.4)			R523 (0.1)	Y623(0.15)
2 (10 mm)	C124 (0.2)	B stack			R524 (0.1)	Y624(0.15)
		B 221 (0.2)	B 32(1.0)	B 42(1.0)		Y625(0.15)
		B 222 (0.2)				
		B 223 (0.5)				
1 (10 mm)	TVA11	TVA21	TVA31	TVA41	TVA51	TVA61
Tip Surface (50 mm)	(1.1)	(1.1)	(1.1)	(1.1)	(1.1)	(1.1)
	V1(0.02)		V3(0.02)	V4(0.02)	V5(0.02)	

Table 1: Overview of samples as they were positioned on the BN sample holder at JET. The shading refers to which laboratory analysed the sample – see in section 2.2.2 - (dark grey- LNGS, light grey-PTB and black-IRMM). The numbers in parenthesis correspond to the thickness of the samples in mm. B: B4C, L: LiF, C: cobalt based alloy (Havar), W: tungsten, V: vanadium, R: rhodium, Y: yttrium, T: titanium and TVA Titanium Aluminium Vanadium: $Ti_{0.9}V_{0.04}Al_{0.06}$.

	Max. Larmor radius at 2.2T (cm)	Max. Larmor radius at 3.4T (cm)
Helium 3 (0.82MeV)	5	3.3
Tritons (1.01MeV)	11	7.4
Proton (3.03MeV)	11	7.4
Alpha (3.67MeV)	12	8
Proton (14.68MeV)	25	16.7

Table 2: Larmor radii of charged fusion products

JET Pulse No:	Toroidal field (T)	Plasma current (MA)	Scintillator light (a.u)	D-D yield [a] (a.u)	D-^{3}He yield[b] (a.u)
72622	3.45	1.8	0.31	0.068	0.086
72624	3.0	1.8	9.27	0.115	0.134
72626	3.0	2.2	1.73	0.066	0.075
72628	3.0	1.5	7.67	0.083	0.082
72629	2.5	1.5	9.73	0.097	0.123
72631	2.5	1.8	7.1	0.112	0.142
72632	2.5	2.2	1.81	0.098	0.127
72633	2.2	1.8	9.08	0.138	0.127
72634	2.2	1.8	0.67	0.105	0.067
72635	2.2	1.8	4.80	0.118	0.037

[a] : fraction of the total 2.5 MeV D-D absolute neutron emission
[b] : relative 16.6 MeV gamma emission

Table 3: List of plasma pulses with ^{3}He gas puffing and including values for the toroidal magnetic field, plasma current, scintillator light, D-D and D-^{3}He fusion reaction yield. Measurements of the charged particle activation probe are time integrated over the 10 JET pulses.

S[a]	RN[b]	PR[c]	Thr[d] (MeV)	Activity (Max-mBq/g)	Samples
TiVAl	$^{48}V_{(t_{1/2}= 15.98d)}$	$^{48}Ti(p,n)$	4.9	840 ± 65	TV11,TV21,TV31,TV41,TV61
	$^{51}Cr_{(t_{1/2}= 27.7d)}$	$^{51}V(p,n)$	1.5	50 ± 25	TV11,TV21
		$^{48}Ti(\alpha,n)$	2.9		
V	$^{51}Cr_{(t_{1/2}= 27.7d)}$	$^{51}V(p,n)$	1.5	673 ± 47	V1
B_4C	$^{7}Be_{(t_{1/2}= 53.3d)}$	$^{10}B(p,\alpha)$	0	91.4 ± 14	B221, B222, B223, B241
LiF	$^{7}Be_{(t_{1/2}= 53.3d)}$	$^{7}Li(p,n)$	1.9	162± 24	L231,L232, L233, L251
Y	$^{89}Zr_{(t_{1/2}= 78h)}$	$^{89}Y(p,n)$	3.7	2751 ± 184	Y621, Y622, Y623, Y624, Y625
Rh	$^{103}Pd_{(t_{1/2}= 16.99d)}$	$^{103}Rh(p,n)$	1.3	725 ± 59	Rh522, Rh524
Co-alloy	$^{52}Mn_{(t_{1/2}= 5.59d)}$	$^{52}Cr(p,n)$	5.6	97 ± 12	Co1,Co2
	$^{56}Co_{(t_{1/2}= 77.7d)}$	$^{56}Fe(p,n)$	5.4	31 ± 6	Co1,Co2

[a] S: Sample
[b] RN: Radionuclide found
[c] PR: Production reaction
[d] Thr: Energy threshold for the reaction

Table 4: Overview of the measured charged particle induced radionuclides.

Sample	R	PR	14.6 MeV proton (10^9 cm^{-2})
TV111	$^{48}V_{(t_{1/2}= 15.98d)}$	$^{48}Ti(p,n)$	1.43 ± 0.11
B223, L233, B241, L251	$^{7}Be_{(t_{1/2}= 53.3d)}$	$^{10}B(p,\alpha)$ $^{7}Li(p,n)$	0.38 ± 0.06*
V1	$^{51}Cr_{(t_{1/2}= 27.7d)}$	$^{51}V(p,n)$	0.94 ± 0.08
C121	$^{56}Co_{(t_{1/2}= 77.7d)}$	$^{56}Fe(p,n)$	0.83 ± 0.15
C121	$^{52}Mn_{(t_{1/2}= 5.59d)}$	$^{52}Cr(p,n)$	0.82 ± 0.1
Y621	$^{89}Zr_{(t_{1/2}=78 h)}$	$^{89}Y(p,n)$	0.28 ± 0.02

Table 5: Values for the 14.6 MeV proton flux measured at several samples, the activation product used and the main production reaction (see in table 2 for detector label). (*) indicates a sum of four detectors.

Charged particle	Simulated flux ($10^9 cm^{-2}$)	Measured flux ($10^9 cm^{-2}$)
α (3.7 MeV)	0.08	< 3.6
p (3.0 MeV)	0.17	0.15+- 0.4

Table 6: Results for alpha particles and d(d,p)t fusion reaction products, respectively comparing simulated and experimental data.

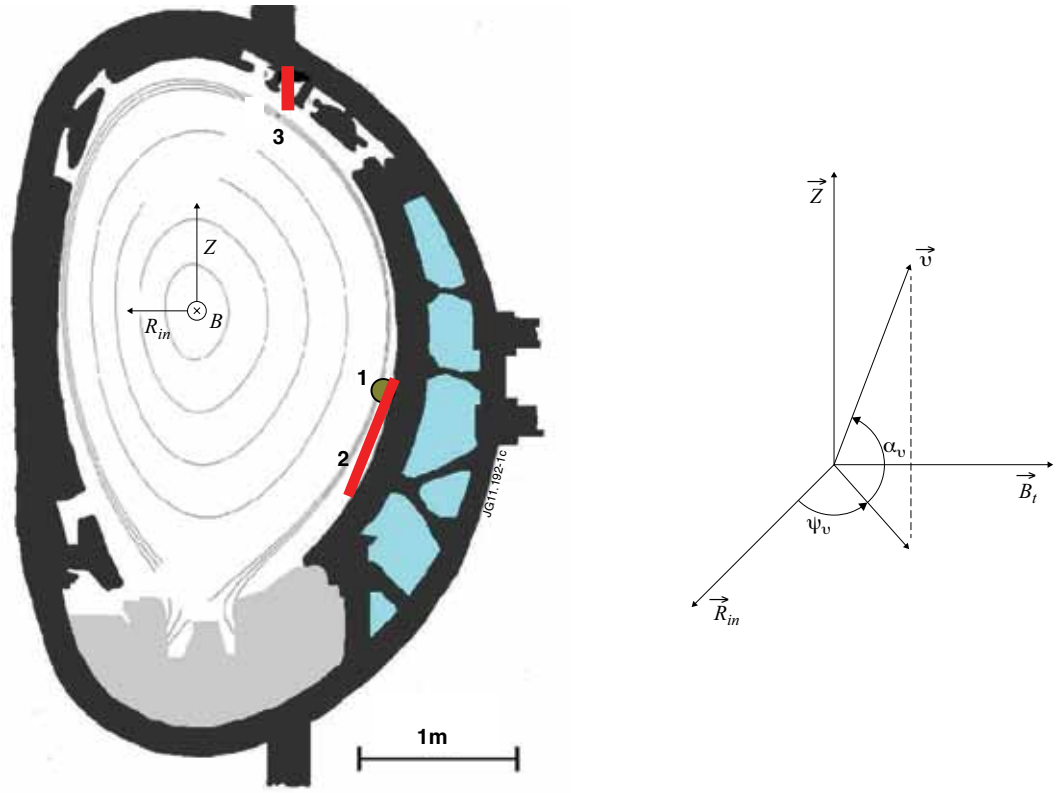

Figure 1: Poloidal cross section across JET tokamak showing the poloidal positions of the three energetic ion loss diagnostics: 1) Scintillator at octant 4 (z= −0.28m, R = 3.80m), 2) Faraday cup array in octant 7 (z = −0.22m to z = −0.80m), 3) activation probe, at octant 5, (R = 3.28m, z= +1.77m). Right, reference coordinate system used to indicate the position and orientation of the charge particle activation probe (see in section 2.2).

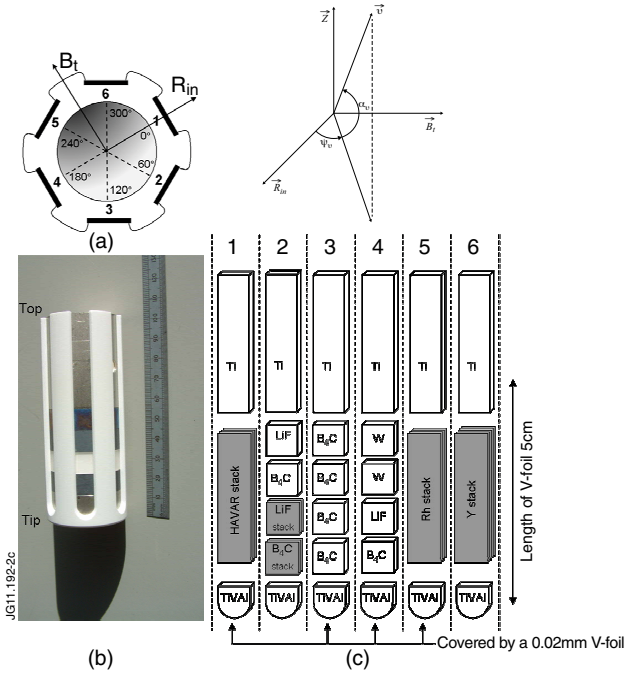

Figure 2. Layout for the charged particle activation probe for JET. a) Six slots for measurement of the activation angular distribution. b) several samples per slot for measurement of the radial profile. c) Five stacks shown in grey for measurement of the depth distribution, providing information on energy. d) Sample position with respect to the tokamak is given in the inset coordinate system (see also in figure 1).

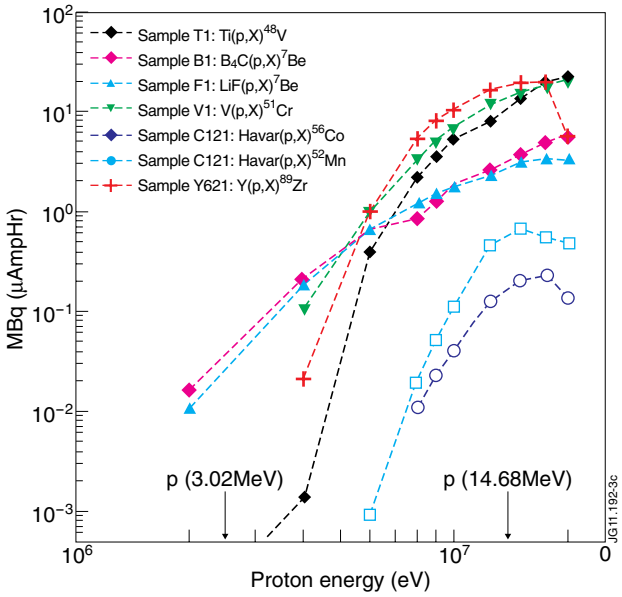

Figure 3: Activation coefficients calculated with FISPACT [29] for several materials irradiated by protons at different energies. The position on the energy axis for D-D and D-^{3}He protons is indicated by an arrow

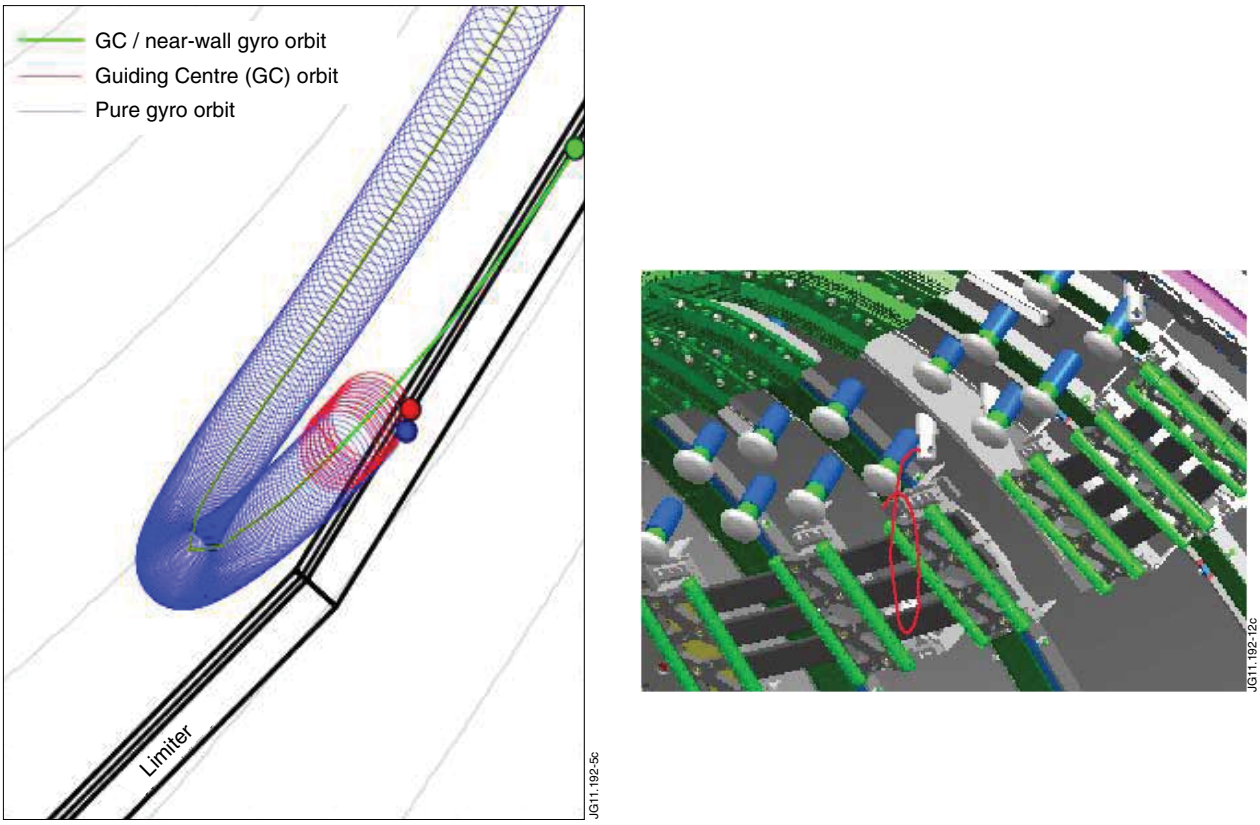

Figure 4 : Left: A schematic drawing of a particle trajectory reaching close to the wall. If the guiding center is followed in the simulation, the particle hits the plasma facing component when the guiding center trajectory intersects the wall (green circle). If the full orbit is followed, the particle hits at a different location (blue circle) and in the 'near wall' mode ASCOT simulation the particle hits at a location (red circle) much nearer to the full orbit simulation[51] (compare green and red circle).

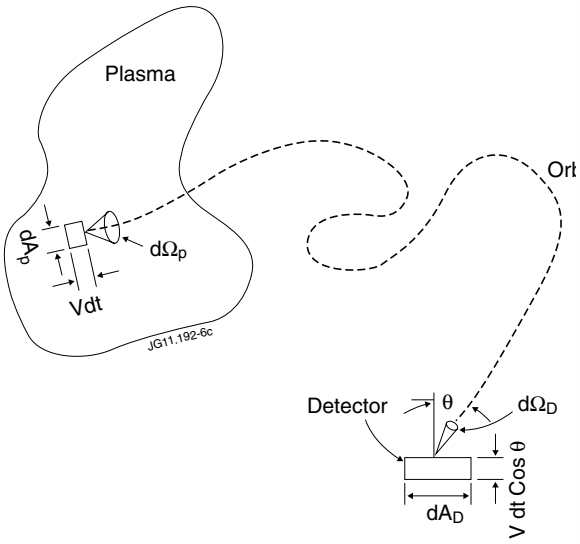

Figure 5: Schematic diagram of the differential volume in phase-space that emits ions into the differential phase-space volume measured by the detector [43].

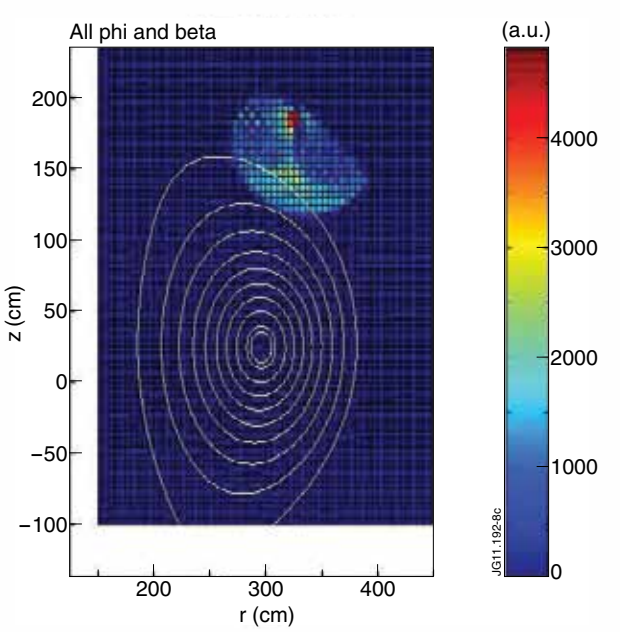

Figure 6: Detection efficiency distribution epsilon e (r, z) plotted in arbitrary units. The 4-D distribution is integrated over the ϕ and β variables for Pulse No: 72624 for 14.6MeV protons.

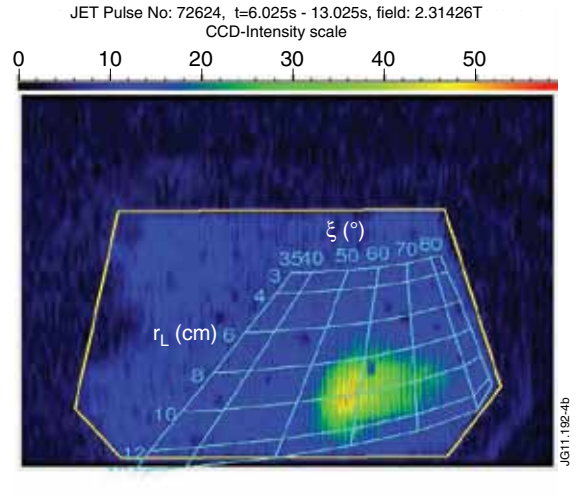

Figure 7: CCD image of the JET scintillator plate[9]. The bi-dimensional grid defines the repective ranges in gyroradius r_L – 3cm to 12cm – and pitch angle ξ – 350 to 800. A typical alpha particle orbit loss signal is plotted for JET Pulse No: 72624.

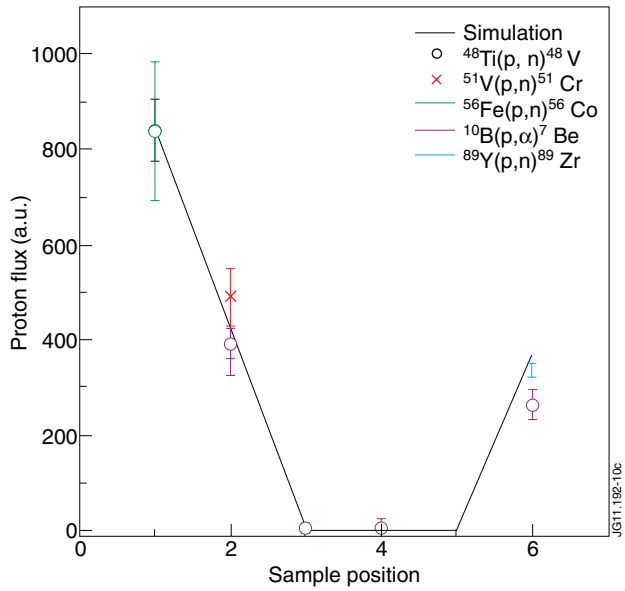

Figure 8: Angular distribution (pitch angle) of fusion product loss. Comparison between simulation and activation data from several proton induced products. A strongly anisotropic distribution is observed.

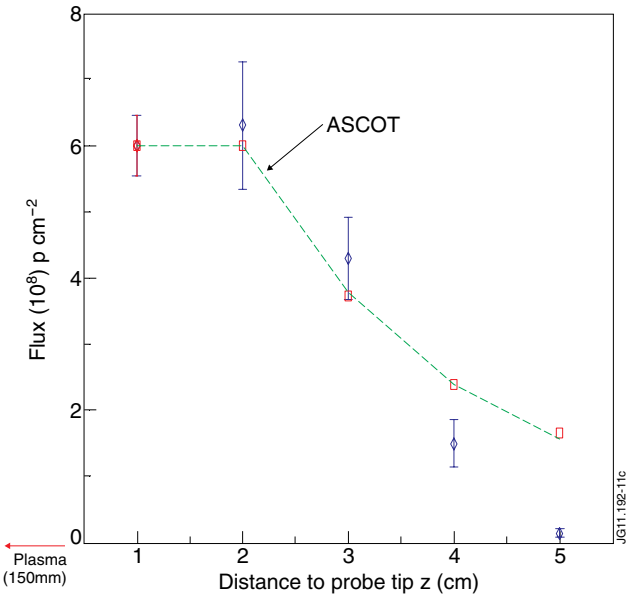

Figure 9: Radial profile of fusion reaction product d(^{3}He,p)α. Comparison between ASCOT simulations (square symbols) and experimental data (diamond symbols). The experimental data are the absolute values for the 14.6MeV proton flux obtained from the slot number 2 samples at $\psi_V = 60^o$. See in figure 1 and figure 2 for ψ_V the orientation of the activation detectors with respect to the tokamak. Note the values for the calculated data are relative.